

Demonstration of Electrostatic MEMS Bifurcation Sensors

M.S. Al-Ghamdi*, M. Khater**, K.M.E. Stewart***, A. Alneamy*, R. Almikhlafl*, S. Park*,
E. M. Abdel-Rahman*, and A. Penlidis***

*Systems Design Engineering, University of Waterloo, Waterloo, Ontario, Canada

**Mechanical Engineering, KFUPM, Dhahran, Saudi Arabia

*** Chemical Engineering, University of Waterloo, Waterloo, Ontario, Canada

Summary. A novel electrostatic MEMS sensor employing a dynamic bifurcation detection technique is demonstrated. The sensor detects ethanol vapor in binary mode, reporting ON-state (1) for concentrations above a preset threshold and OFF-state (0) for concentrations below the threshold. The sensing mechanism exploits the qualitative difference between the sensor state before and after dynamic pull-in. Experimental demonstration was carried out using a laser Doppler vibrometer to measure the sensor motion in time and frequency domains. The sensor was able to detect 1 ppm of ethanol vapor in dry nitrogen within 22 seconds.

Introduction

Micro-mass sensors have been widely used as sensing platforms for inertial gas sensors in chemical, medical and automotive application [1]. The sensor is coated with a highly selective detector material to capture a target gas. They detect the presence of the gas in ambient air as a small variation in the sensor mass, on the order of nano- to atto-gram [2, 3]. The response of gas sensors can be measured optically [4], capacitively [5], or piezoresistively [6]. Optical readout is more accurate but less practical than other measurement techniques. MEMS gas sensors have been developed; however, they have significant challenges, such as stability, detection range, response time, hysteresis, power consumption, reliability and cost effectiveness [7].

The two commonly used detection modes in gas sensors are static and dynamic sensing. The static mode measures mass sorbed onto the polymeric sensing material as a change in structural displacement [6]. In the dynamic sensing mode, the sensor measures the shift in one of its resonant frequencies induced by a mass sorbed onto a detector material [3]. The sensitivity of dynamic sensing is higher than that of static (or forced) sensing by 1-2 orders of magnitude [8, 9]. Therefore, it has the ability to increase absolute mass detection, on the order of atto-grams, and can be utilized to realize highly sensitive sensors [10].

A class of inertial sensors seeks to use bifurcations to enhance sensor sensitivity [11, 12, 13]. Zhang et al. [8] exploited a subcritical pitchfork bifurcation in a electrostatic comb-finger sensor to detect water vapor using platinum (Pt). A laser Doppler vibrometer (LDV) was used to measure 0.7 pg of water vapor. Li et al. [14] employed a supercritical pitchfork bifurcation in a piezoelectric actuated beam sensor to detect 2,4 DNT. They detected electrically a concentrations of 1.38 ppb. Nayfeh and co-workers [12] proposed sensors based on shift in the location of static and dynamic bifurcations. We demonstrated experimentally that a binary gas sensor based on a static bifurcation can detect 5 ppm of ethanol in dry nitrogen (a mass of 165 pg) [15, 16].

In this work, we present a binary gas sensor based on a dynamic bifurcation to detect ethanol vapor in dry nitrogen. The cyclic-fold bifurcation in an electrostatic MEMS sensor is used to create the discrete (binary) output states.

Sensor Design

The sensor was fabricated using the PolyMUMPs fabrication process [17]. It features a cantilever beam fabricated in Poly2 structural layer with the structural dimensions: $175 \times 10 \times 1.5 \mu\text{m}$. The material properties are $\rho = 2300 \text{ kg/m}^3$ and $E = 160 \text{ GPa}$, Fig. 1. The gap underneath it is etched in second oxide layer resulting in a gap distance of $d = 2 \mu\text{m}$,

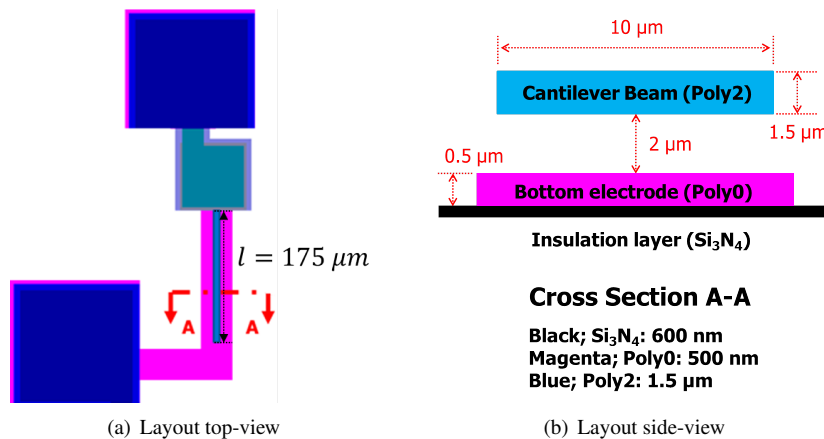


Figure 1: Schematics of the PolyMUMPs fabricated gas sensor

Fig. 1(b). A polysilicon electrode is patterned in Poly0 layer directly under the beam to act as a ground electrode. The ground electrode overlaps with the full length of the beam. Two gold pads are patterned at the root of the beam and the end of the bottom electrode to apply potential difference between them. The pads are also used to drive a current through the semi-conductor polysilicon structure to reset the sensor via Joule heating.

Detection Mechanism

The sensor exploits the qualitative change before and after a dynamic bifurcation in electrostatic MEMS, dynamic pull-in, as a sensing mechanism. It is used in this study as a binary logic gate where the system can either, detect (high) or not detect (low) the presence of a target gas.

The sensor is actuated by a combination of AC-DC voltage between the beam and a fixed electrode. The operating conditions (excitation frequency f_o , amplitude V_{ac} and bias voltage V_{dc}) are set to allow a large enough basin of attraction for the beam periodic oscillations, thereby protecting against external disturbances driving it across the bifurcation point and leading to a false positive (detection signal in the absence of ethanol vapor).

A frequency sweep of the actuation voltage is implemented to obtain the frequency-response of the sensor and to identify the location of the dynamic pull-in, f_{pi} . The mass added by ethanol molecules sorbed to the detector polymer will cause a jump and trigger pull-in. The magnitude of the set-off frequency, $\delta f = f_{pi} - f_o$, determines the size of the critical mass and the threshold ethanol concentration required to trigger a detection signal; dynamic pull-in. The sensor impedance before and after the jump represent the low and high states of the logic gate, respectively. We note that as the set-off frequency is decreased, the sensitivity will be enhanced. We used a laser Doppler vibrometer (LDV) to confirm the transition between the sensor states.

Sensor Model

The gas sensor is actuated under a quasi-electrostatic MEMS actuator. It consists of a microcantilever beam vibrating in z-direction, as shown in Fig. 2(a). The beam length, width, and thickness are denoted l , b , and h , respectively. The cantilever beam is coated with a detector polymer, coupled to an electrode located at a distance d underneath it, and actuated by AC and DC voltage, Fig. 2(b). The model of this sensor is developed based on Newton's second law, which describes the

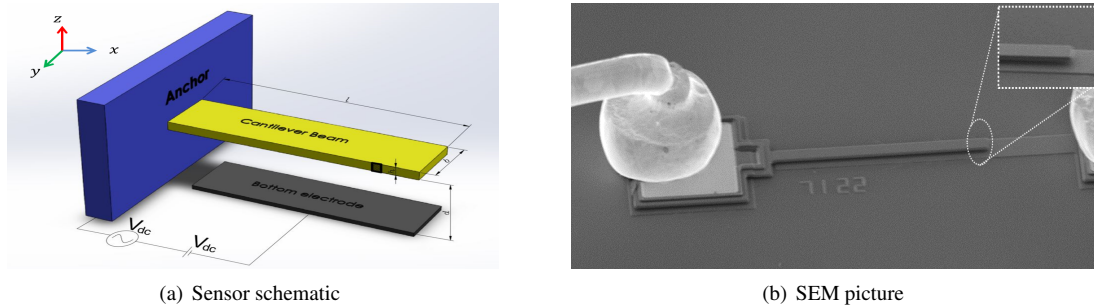


Figure 2: Gas sensor

dynamic behavior of the system. It treats the microbeam as an elastic continuum and prismatic, an Euler-Bernoulli beam. The non-dimensional equation of motion can be described as

$$\ddot{w} + (c + c_s)\dot{w} + w^{iv} - \alpha_1 w'' \int_0^1 (w'')^2 dx = \alpha \left(1 + 0.65 \frac{1-w}{\frac{b}{d}}\right) \frac{(V_{dc} + V_{ac})^2}{(1-w)^2} \quad (1)$$

the associate boundary conditions are

$$\begin{aligned} w(0, t) = 0 \quad \text{and} \quad w'(0, t) = 0 \\ w''(1, t) = 0 \quad \text{and} \quad w'''(1, t) = 0 \end{aligned} \quad (2)$$

where parameters are defined as

$$\begin{aligned} \alpha = \frac{\varepsilon b L^4}{2EI d^3}, \quad c = \frac{\hat{c} L^4}{EIT}, \quad \alpha_1 = 6 \left(\frac{d}{h}\right)^2, \quad T = \sqrt{\frac{\rho A L^4}{EI}} \\ \mu = \hat{\mu} \left(\frac{b}{d}\right)^3 \frac{T}{m}, \quad c_s = \frac{\mu}{(1 + 6K_n)(1-w)^3} \end{aligned} \quad (3)$$

The squeeze-film damping coefficient, in addition, was expanded and accounted for one factor only using Taylor series expansion as follow:

$$c_s \approx (\mu_e + \mu_e w) \frac{1}{(1-w)^2} \quad \text{where} \quad \mu_e = \frac{\mu}{1 + 6K_n} \quad (4)$$

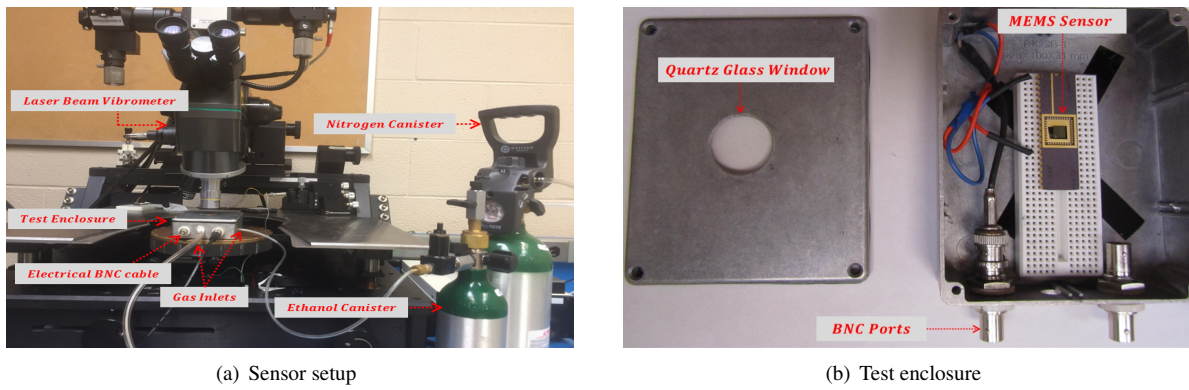
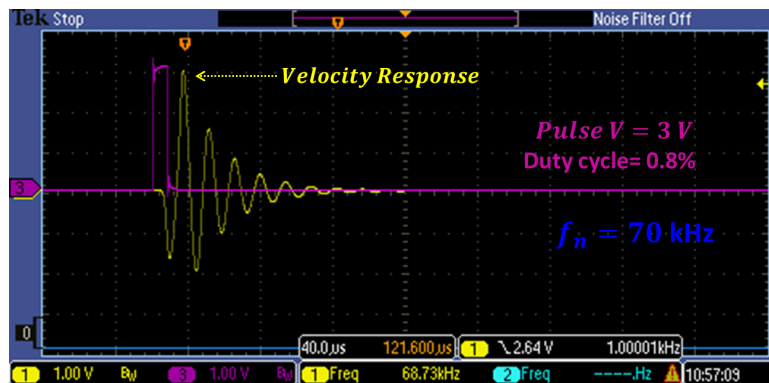


Figure 3: Experimental setup

Sensor Demonstration

The experimental setup, Fig. 3(a), is composed of the sensor placed inside a test enclosure, a function generator, a high voltage amplifier, an oscilloscope, and two gas canisters containing nitrogen gas (5.0 grade) and pre-calibrated ethanol gas in a balance of nitrogen. A laser Doppler vibrometer is used to measure sensor responses optically. The test enclosure shown in Fig. 3(b) (volume 44,253 cm³) was designed to control the composition of the gas mixture to which the sensor is exposed. The chamber is equipped with a BNC port to connect the sensor to the function generator and a quartz glass window to allow optical access for the laser beam of the vibrometer.

The damped natural frequency and quality factor were measured optically in atmospheric pressure by applying a pulse train with an amplitude of 3 V, a frequency of 1 kHz, and a 0.8% duty cycle, Fig. 4. An average of 512 samples of the velocity time-history was captured from the oscilloscope. The damped natural frequency was found to be $f_d = 70$ kHz. The quality factor was obtained using the half-power method ($Q = \frac{f_n}{\Delta f}$) as $Q = 5.4$. The settling time was measured as $t_s = 80 \mu\text{s}$.


 Figure 4: The averaged velocity time-history under a pulse train with a frequency of $f = 1$ kHz and amplitude of 3 V

Poly 2,5-dimethyl aniline (P25DMA), a polymer with affinity to ethanol vapor [18], was deposited manually onto the beam top surface, Fig. 5(a). Four drops of polymer-glycerol solution were deposited atop the outer half of the beam length, Fig. 5(b). Glycerol was allowed to naturally evaporate in air leaving the polymer residue on the beam, Fig. 5(c). The sensor was characterized again after deposition. No significant difference was found in the natural frequency or quality factor.

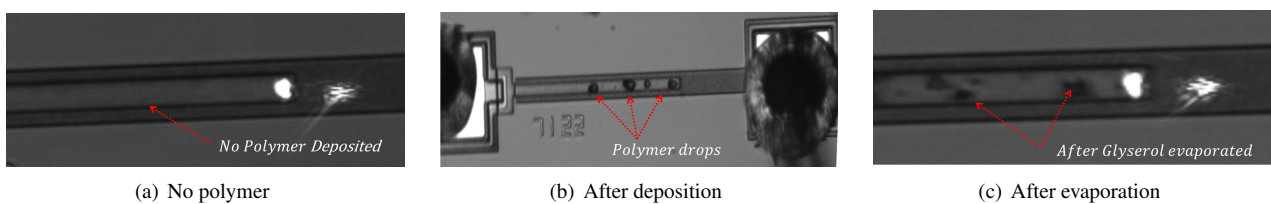


Figure 5: The sensor (a) before deposition (b) right after deposition of polymer solution and (c) after evaporation of solvent

Dynamic Pull-in

The laser Doppler vibrometer [19] was utilized to characterize the dynamic response of the beam under electrostatic force over a wide frequency range. A combined AC-DC voltage with a modulation index of one, $V_{dc} = V_{ac}$, was utilized to locate the cyclic-fold bifurcation. The sensor was characterized using forward and backward frequency sweeps over the frequency range $f = [50-90]$ kHz to generate the frequency-response curve. The bias voltage and excitation amplitude were set to $V_{dc} = V_{ac} = 7.446$ V. A slow slew rate of $f = 2.5$ kHz/s was used to minimize transient effects. Data were collected using an oscilloscope in time windows of 0.4 s each and a sampling rate of $f_s = 313$ kHz. The frequency-response curve, Fig. 6, was obtained by post-processing the data to evaluate the RMS of the beam tip velocity over a time window of $20T$ and assigning it to the frequency value at the window mid-point.

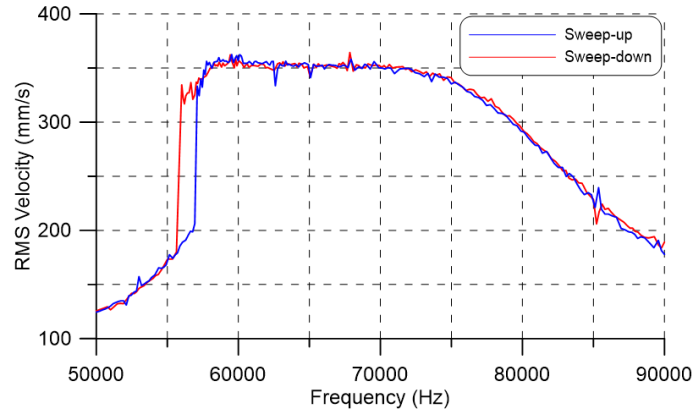


Figure 6: The measured frequency-response curve for $V_{dc} = V_{ac} = 7.446$ V. Forward sweep shown in blue colored line and backward sweep shown in red colored line

The forward sweep is shown in blue solid line and the backward sweep in red solid line in Fig. 6. The jump-up during the forward sweep at $\Omega = 56.810$ kHz corresponds to the lower cyclic-fold bifurcation. The jump-down during the backward sweep at $\Omega = 55.986$ kHz corresponds to the upper cyclic-fold bifurcation. The region between the two jumps demarcates hysteresis in the sensor response. The flatness in the left branch of the curve is due to the presence of (nonlinear) squeeze-film damping.

Experimental Results

A series of experiments were conducted to determine the minimum detectable ethanol concentration (detection limit) for sensors with P25DMA. The test gases were 5 ppm and 1 ppm ethanol vapor in dry nitrogen under its own pressure, $P = 20$ psi. The operating point of the sensor is set to a frequency f_o just below the cyclic-fold bifurcation. We define the set-off frequency as the difference between the bifurcation point frequency f_{pi} and the operating frequency:

$$\delta f = f_{pi} - f_o$$

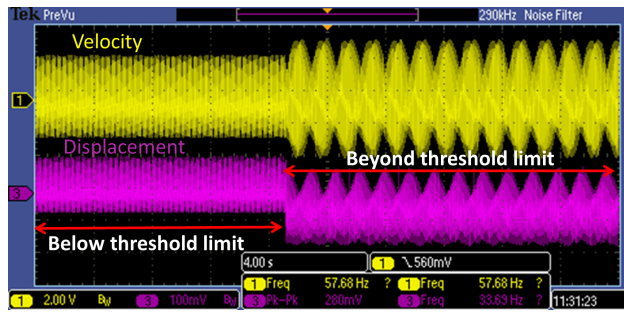
A manual frequency sweep-up was carried out with a frequency step of 1 Hz to determine the location of the bifurcation point precisely f_{pi} . A stability study was then carried out to determine the closest stable position under ambient external disturbances by stepping back from f_{pi} in steps of 1 Hz. The point where the operating conditions can be sustained for longer than 15 minutes was declared stable. The smallest stable set-off frequency for the current sensor and experimental setup was found to be $\delta f = 2$ Hz.

Experiment # 1:

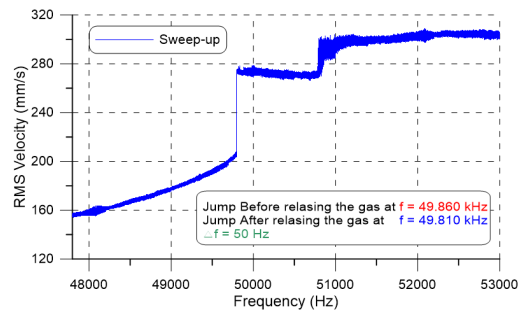
After purging the test chamber with dry nitrogen for 15 minutes, a mixture of 5 ppm ethanol vapor in dry nitrogen was slowly released into the chamber. The operating frequency was initially set to $f_{pi} - 160$ Hz and increased in steps of 10 Hz with a hold-off period of 300 s after each step. The hold-off period is eight orders-of-magnitude higher than the settling time, $t_s = 80 \mu s$, guaranteeing elimination of transient effects. Detection (dynamic pull-in) occurred at a set-off frequency of $\delta f = 50$ Hz within one second of frequency change. Fast detection indicates that the sorbed mass is well beyond the sensor threshold at this operating point ($f_o - 50$ Hz). It resulted in shifting the cyclic-fold bifurcation well below the operating point.

The jump in the sensor response was observed in the amplitude and envelope of the velocity and displacement time-histories were recorded using the oscilloscope, Fig. 7(a). These show a jump in amplitude and irregularity of the time-envelope indicating the presence of higher harmonics. The experiment was repeated twice to ensure repeatability of detection.

After detection, a forward frequency sweep was carried out over the frequency range $f = [47.8, 53]$ kHz, Fig. 7(b). It captures the jump-up at $f = 49.810$ kHz compared to its original location before gas release measured precisely at $f = 49.860$ kHz. We note that the right branch of the frequency response curve features a step up in velocity at $f = 50.8$ kHz



(a) The sensor velocity (yellow) and displacement (magenta) time-histories before and after 5 ppm ethanol detection



(b) The velocity frequency-response curve after ethanol mixture release

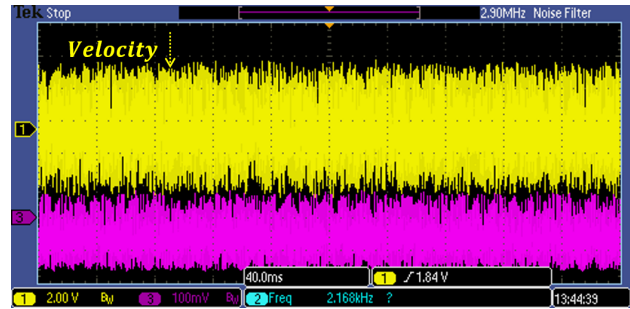
Figure 7: The sensor response before and after detection of 5 ppm ethanol

while increasing the frequency. The larger-sized orbits on the right branch correspond to in-air oscillations similar to those seen in Fig. 6. The mid-sized orbits observed right after the jump-up correspond to tapping-mode oscillations involving the sensor tip interaction with the bottom electrode. The higher harmonics detected in the time-envelope of the velocity and displacement, Fig. 7(a), indicate the presence of impacts within those orbits, consistent with tapping-mode oscillations. We note that tapping does not destroy the sensor. While it produces intermittent oscillations, it rarely results in stiction.

Experiment # 2:



(a) Before releasing ethanol



(b) After releasing ethanol

Figure 8: The sensor velocity (yellow) and displacement (magenta) time-histories of 1 ppm ethanol detection

A mixture of 1 ppm ethanol vapor in dry nitrogen was slowly released into the chamber. The set-off frequency was again set to $\delta f = 50$ Hz. Detection (dynamic pull-in) occurred after 22 seconds from gas release. The length of time required for detection indicates that the sorbed mass was small enough to move the cyclic-fold bifurcation point just below the operating frequency f_o . Therefore, 1 ppm ethanol is very close to the sensor detection threshold at this operating point. The velocity and displacement time-histories of the sensor before and after detection were recorded using an oscilloscope, Fig. 8. Comparing the two figures shows a significant increase in amplitude and irregularity of the time-envelope indicating the presence of higher harmonics.

Discussion

The minimum detectable gas concentration is dependent on the minimum realizable set-off frequency δf and the type and distribution of the detector polymer coat on the sensor surface. No attempt was made to optimize these factors, since the purpose of this study is limited to feasibility demonstration.

Compared to the static binary sensor [15, 16], the dynamic binary sensor response was faster (1 s compared to 7 s) for the same gas concentration (5 ppm of ethanol). It was also more sensitive, detecting 1 ppm of ethanol vapor at a set-off frequency of $\delta f = 50$ Hz, much larger than its minimum value ($\delta f = 2$ Hz), while the set-off voltage of the static binary sensor was at its minimum value ($\delta V = 1$ mV). Linear extrapolation suggests that the minimum detectable concentration of the dynamic binary sensor may be as low as 40 ppb. While linear theory suggests that dynamic detection is more sensitive than static detection, it attributes that to dynamic amplification and limits sensitivity enhancement to the same order as the sensor quality factor ($Q = 5.4$). This would have suggested a detection limit of 1 ppm. The difference between these two levels is due to the superior sensitivity achieved via bifurcation-based sensing.

We note that all experiments were conducted in air on a probe station that was not isolated from ground vibrations. Not only were no precautions taken to protect the sensors against external disturbances, but also deliberate attempts were made to disturb them via impacts to the probe station. However, no false positives were detected in any of the experiments conducted on this sensor. These anecdotal observations indicate that the stability of MEMS inertial sensors against

external disturbances is significantly better than that of macro-sized inertial sensors because of their minute masses.

Conclusion

We utilized a novel detection mechanism that exploits the qualitative change in electrostatic MEMS sensors state before and after a dynamic bifurcation, dynamic pull-in, to implement binary gas sensors. A biased AC waveform was used to excite the sensor and maintain it close to the cyclic-fold bifurcation. Added mass due to sorbed gas molecules was allowed to trigger the bifurcation, thereby maximizing the sensor sensitivity. The sensor indicates that the ambient ethanol concentration has exceeded the threshold by going into the dynamic pull-in, thereby sending a binary detection signal. Our implementation shows that this sense mechanism has the advantage of reducing requirements on readout electronics while enhancing sensitivity and robustness. Specifically, the dynamic binary ethanol sensor was able to detect 1 ppm ethanol in dry nitrogen at a set-off frequency of $\delta f = 50$ Hz.

Acknowledgment:

The authors acknowledge the support of National Sciences and Engineering Research Council of Canada (NSERC). Also, the first author acknowledges the support of King Abdulaziz City for Science and Technology (KACST).

References

- [1] Park, K., Kim, N., Morissette, D.T., Aluru, N.R., and Bashir, R. (2012) Resonant MEMS mass sensors for measurement of microdroplet evaporation. *Journal of Microelectromechanical Systems*, 21(3), pp.702-711.
- [2] Ilic, B., Yang, Y., and Craighead, H.G. (2004) Virus detection using nanoelectromechanical devices. *Applied physics letters*, 85(13), pp.2604-2606.
- [3] Pikul, J.H., Graf, P., Mishra, S., Barton, K., Kim, Y.K., Rogers, J.A., Alleyne, A., Ferreira, P.M., and King, W.P. (2011) High precision electrohydrodynamic printing of polymer onto microcantilever sensors. *IEEE Sensors Journal*, 11(10), pp.2246-2253.
- [4] Xie, H., Vitard, J., Haliyo, S., and Régnier, S. (2008) Enhanced sensitivity of mass detection using the first torsional mode of microcantilevers. *Measurement Science and Technology*, 19(5), p.055207.
- [5] Dohn, S., Hansen, O., and Boisen, A. (2006) Cantilever based mass sensor with hard contact readout. *Applied Physics Letters*, 88(26), p.264104.
- [6] Zhu, W., Park, J.S., Sessler, J.L., and Gaitas, A. (2011) A colorimetric receptor combined with a microcantilever sensor for explosive vapor detection. *Applied Physics Letters*, 98(12), p.123501.
- [7] Thundat, T., Oden, P.I., and Warmack, R.J. (1997) Microcantilever sensors. *Microscale Thermophysical Engineering*, 1(3), pp.185-199.
- [8] Zhang, W., and Turner, K. L. (2005) Application of parametric resonance amplification in a single-crystal silicon micro-oscillator based mass sensor. *Sensors and Actuators A: Physical*, 122(1), 23-30.
- [9] Younis, M.I., and Alsaleem, F. (2009) Exploration of new concepts for mass detection in electrostatically-actuated structures based on nonlinear phenomena. *Journal of computational and nonlinear dynamics*, 4(2), p.021010.
- [10] Waggoner, P.S., and Craighead, H.G. (2007) Micro- and nanomechanical sensors for environmental, chemical, and biological detection. *Lab on a Chip*, 7(10), pp.1238-1255.
- [11] Khater, M.E., Abdel-Rahman, E.M., and Nayfeh, A.H. (2009) A mass sensing technique for electrostatically-actuated mems. *ASME 2009 International Design Engineering Technical Conferences and Computers and Information in Engineering Conference*, pp. 655-661.
- [12] Khater, M. E., Abdel-Rahman, E. M., and Nayfeh, A. H. (2010) Methods and Systems for Detection Using Threshold-Type Electrostatic Sensors. *U.S. Patent Application No. 12/791, 293*.
- [13] Rhoads, J.F., Shaw, S.W., and Turner, K.L. (2010) Nonlinear dynamics and its applications in micro- and nanoresonators. *Journal of Dynamic Systems, Measurement, and Control*, 132(3), p.034001.
- [14] Li, L.L., Holthoff, E. L., Shaw, L. A., Burgner, C. B., and Turner, K. L. (2014) Noise squeezing controlled parametric bifurcation tracking of MIP-coated microbeam MEMS sensor for TNT explosive gas sensing. *Journal of Microelectromechanical Systems*, 23(5), 1228-1236.
- [15] Khater, M. E., Al-Ghamdi, M., Park, S., Stewart, K. M. E., Abdel-Rahman, E. M., Penlidis, Nayfeh, A. H., Abdel-Aziz, A. K. S., and Basha, M. (2014) Binary MEMS gas sensors. *Journal of Micromechanics and Microengineering*, 24(6), 065007.
- [16] Alghamdi, M. 2015 Inertial MEMS Sensors. Master thesis, *University of Waterloo*.
- [17] Koester, D., Cowen, A., Mahadevan, R., Stonefield, M., and Hardy, B. (2003). *PolyMUMPs design handbook*. MEMSCAP Inc.
- [18] Stewart, K.M., Chen, W.T., Mansour, R.R. and Penlidis, A. (2015) Doped poly (2,5-dimethyl aniline) for the detection of ethanol. *Journal of Applied Polymer Science*, 132(28).
- [19] Polytec Inc., OFV-5000 Vibrometer Controller User Manual. www.polytec.com.